Characterization of Flow Distribution in Microchannel Reactors

P. Pfeifer, A. Wenka, and K. Schubert
Institute for Micro Process Engineering, Forschungszentrum Karlsruhe GmbH, POB 3640, 76021 Karlsruhe, Germany

M. A. Liauw and G. Emig
LTC 1, University Erlangen-Nürnberg, Egerlandstrasse 3, 91058 Erlangen, Germany

The applicability of thermal anemometry with constant wire temperature for characterization of the flow distribution in microchannel reactors was first proven by a comparison of simulation and experimental results using uncoated microchannels. The anemometry was then applied for structured reactor foils with different nanoparticle washcoats. Homogeneity of the coatings observed by scanning electron microscopy showed good correlation to the results of the anemometry. © 2004 American Institute of Chemical Engineers *AIChE J,* 50: 418–425, 2004

Keywords: hot wire anemometry, constant temperature anemometry, microchannel reactor, microstructure reactor, flow distribution, methanol-steam reforming, nanoparticle washcoat, layer thickness

Introduction

Metallic microstructured/microchannel heat exchangers, or reactors with high heat transfer surfaces and heat transfer coefficients, have a high potential for the safe operation of highly exothermic or endothermic processes (Bier et al., 1990; Schubert et al., 1998). An economically relevant reaction is the steam reforming of methanol, particularly for on-board hydrogen generation in fuel-cell vehicles. Low weight and fast dynamics are the main prerequisites, both of which are excellently met by microsystems (see also Wegeng et al., 1999).

Metallic surfaces and small dimensions turn out to be critical issues (Fichtner et al., 1999; Pfeifer et al., 1999; 2002). In addition, the heterogeneously catalyzed reaction makes it necessary to apply catalyst coatings to the microchannel walls. The studies so far suggest that the catalyst layers should be rather thick. However, with common multichannel microreactors, another critical issue is a well-defined residence time. Every microchannel may be taken as a small single reactor. Obviously, different diameters would lead to different residence times. Applying the catalyst layers now has a finite tolerance. Hence, it is a crucial question how uniform the flow distribution is in an actual multichannel reactor.

SEM pictures of the coatings (Pfeifer et al., 2002), or cutting the microstructured foils and analyzing the distribution of the layer thickness (Pfeifer et al., 1999) can only give a qualitative impression about the coating uniformity. In addition, these methods can only be applied *before* the structured foils are assembled to a complete reactor.

Flow distribution has been made more uniform by the introduction of regions with high pressure drop (see, for example, Ajmera et al., 2001). In applications such as onboard steam reforming, the introduction of high-pressure drops is rather prohibitive. In addition, even at uniform coating thickness, the distribution of the inlet stream across the various channels may be intrinsically nonuniform (Commenge et al., 2002).

An attempt has been made to gauge the degree of flow nonuniformity in monolith channels by *postmortem* measurement, with the lead deposition as an indicator of the local flow rate (Howitt and Sekella, 1974). However, this is only an indirect approach and requires very special conditions. A more general method is needed.

Therefore, a new contact free scanning method at the outlet of the reactors has been developed for the determination of the

Correspondence concerning this article should be addressed to P. Pfeifer at pfeifer@imvt.fzk.de.

Table 1. Summary of Different Preparation Parameters for the Catalyst Layers Examined

Sample	Disperser	Dispersing Time (h)	Drying Temperature	Theoretical Layer Thickness (μm)
A	Magnetic Stirrer	24	ambient	10
B	Ultra Turrax	2	ambient	10
C	Magnetic Stirrer	24	ambient	20
D	Magnetic Stirrer	3	ambient	20
E	Magnetic Stirrer	24	90°C	20

integral volume flow of each microchannel. Hot wire anemometry was considered a reasonable candidate for this characterization.

Experimental

Washcoating of microstructures with nanoparticles

The preparation technique used for preparing thick layers was a washcoating with nanoparticles (for details, see Pfeifer et al., 1999, 2002). Commercially available nanoparticles (20–80 nm dia.) were dispersed in a solution of hydroxy ethyl cellulose (HEC) in water.

When a magnetic stirrer was used for dispersing, 20 wt. % particles were added to a 1 wt.% HEC/water solution and stirred at 1,100 rpm for 3 or 24 h. In cases where an Ultra Turrax T25® from IKA Staufen was used for dispersing, only 10 wt.% particles were added to a 0.5 wt.% HEC/water solution and stirred at 19,000 rpm for 2 h. Subsequent drying (evaporation of water) was performed at ambient temperature or 90°C.

A catalyst loading of about 9.4×10^{-3} g per 10 mm length of the structured aluminum foils (80 channels with a cross section area of 0.1×0.1 mm^2 each and 0.05 mm fins) is equivalent to a layer thickness of approximately 0.01 mm, assuming a homogeneous layer.

The nanoparticle mixture used in all cases consisted of CuO and ZnO with a weight ratio of 1. A summary of all different preparation parameters of the examined layers can be found in Table 1.

Anemometry setup and experimental proceeding

The setup for anemometry (Figure 1) consisted of a clamping device for one structured foil which was connected to a mass-flow controller (Brooks) with a maximum air flow of 7.5 L/min STP on the back of the test equipment. Although small pressure gradients in the gas inlet and high-pressure gradients in the microchannels would result in an equal flow distribution over all the channels (assuming there is no variation in the channel diameter), the inlet tube diameter was the same as the structured foil to prevent effects on flow distribution by the inlet (Figure 2). The device was fixed on a table by a cover plate with slotted holes for precise alignment with respect to the hot wire (Disa). The wire itself had a diameter of 0.005 mm and 2 mm length. It could be positioned (also see Figure 2) by moving the table in y- (along channels exits) and x- (distance to the hot wire) direction with micrometer screws. The height was adjusted by another set screw. The wire position was controlled with an endoscope. A thread transmitted the power of a slow turning motor with additional gear reduction for constant

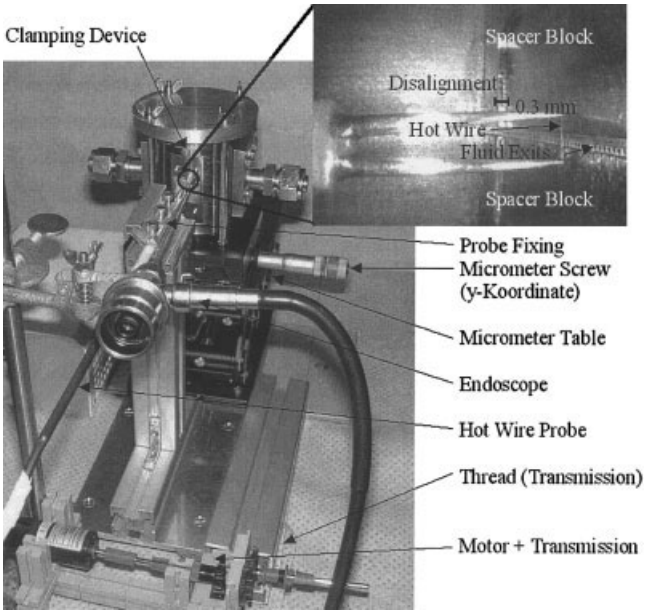

Figure 1. Anemometry equipment with clamping device mounted on a micrometer table; detailed view on the fluid exits and the hot wire.

movement of the table to the y-screw. Together with an AD converter and a LabView® program running on a PC, it was possible to get a voltage value from the Wheatstone bridge (Disa 5120) every 0.004 mm, which was a median value from four single measurements

The fluid exits protruded by 0.3 mm with respect to the clamping device. The $x = 0$ position was set with the micrometer screw, thus by decreasing the distance between the hot wire and channel exits just until a slight bending of the wire was observed. After about 60 min of warm up time, the Wheatstone bridge (280°C wire temperature) displayed a stable voltage signal. The PC program was started, saving the voltage value at zero flow. Then a constant mass flow of 0.5 L/min STP was established. The motor was then started for the scan from $y = 0$ mm to $y = 7$ mm. Thus, the zero flow signal was determined again to demonstrate the stability of the electric

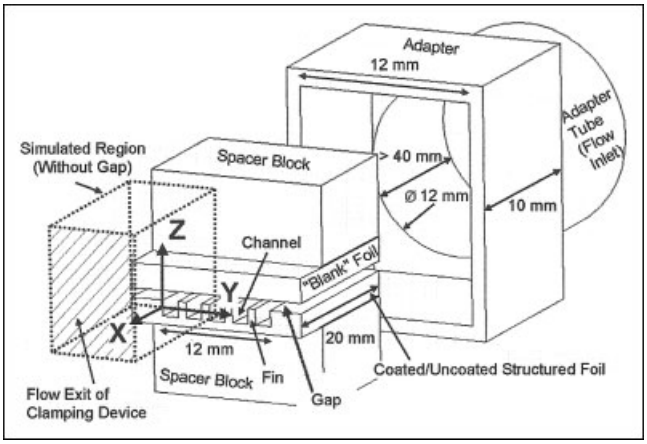

Figure 2. Microsystem, the inlet, and the definition of axes and simulated area.

devices. The distance in the x-direction was determined, revealing a deviation of less than $\pm$ 0.01 mm over the whole range of y. The voltage signal was normalized as follows

$$U_{norm}(y) = \frac{U(y) - U_0}{U_{\max} - U_0} \quad (1)$$

It was verified that this value depended on the flow rate in a linear manner.

Results

Flow simulation

The flow simulation was performed for uncoated channels and for the fluid properties of air with the commercial software package FLUENT®. Assuming the boundary condition of continuum mechanics in the microchannels (Knudsen number is well below 0.01 under ambient conditions in the examined channel diameter), the equations of mass and impulse (Navier-Stokes) balance were solved for flow in the channels. Laminar flow can be assumed because the Reynolds number is only 200. In the outlet region where the diameter is increasing extremely, high fluid velocities of 6 to 30 m/s (depending on the volume flows, see below) at the middle of the channel exit will certainly produce local turbulence. However, in most cells of the simulated exit region (see Figure 2) the flow will also be laminar. Therefore, the k-ϵ RNG model supplied together with FLUENT® was used. This model is a modified version of the usual k-ϵ turbulence model which is recommended for small turbulence regions (see later for a comparison with the experimental data). Due to the symmetry of the simulation region (without a possible gap, see Figure 2), the efficiency could be enhanced by treating one-fourth of that region. Influences of the outlet geometry on the flow distribution were considered to be useful, instead of the simulation of one channel with periodic boundary conditions. Hexahedral cells (12.5 μm/8.35 μm/15 μm) were used for every channel. The length of the channels in the simulation was 1 mm to get a steady flow profile at the exit of the channel. Starting from the channel exits to the flow exit of the clamping device where small flow densities ($\dot{V}$ per cell) were supposed, a tetrahedral cell system with a gradual increase in cell size was used. The error of simulation due to the use of a limited number of cells was calculated to be smaller than 4.5% compared to infinitesimally small cells. The calculation of the maximum error was done by applying up to 20 $\times$ 20 cells in the flow cross section in the laminar flow region directly at the one channel exit. The difference in the flow was observed to bisect at each doubling of the cell number. From the small error it can be concluded that the physics are described well.

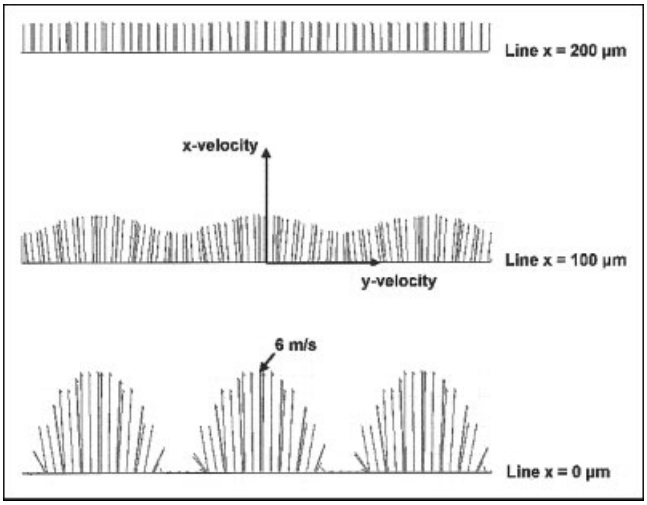

Figure 3. Velocity vectors at half height (z = 0 μm) of the channels for 0, 100, 200 μm distance to the channel exits (x-coordinate) for a total flow of 0.15 L/min STP and 0.05 mm fins between the channels; maximum in vector length corresponds to 6 m/s (simulation).

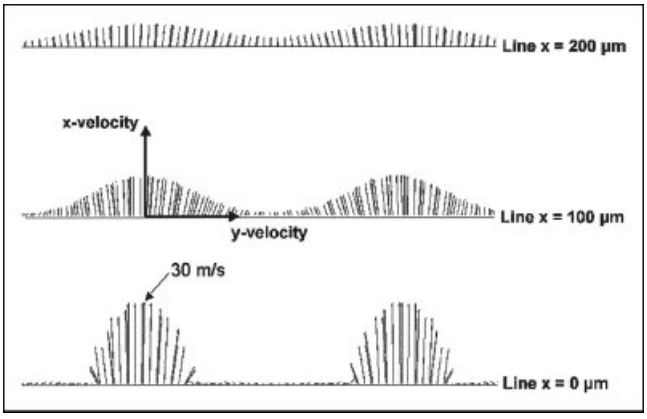

Figure 4. Velocity vectors at half height (z = 0 μm) of the channels for 0, 100, 200 μm distance to the channel exits (x-coordinate) for a total flow of 0.375 L/min STP and 0.2 mm fins between the channels; maximum in vector length corresponds to 30 m/s (simulation).

In the first step the velocity which is proportional to the overall gas flow was varied to obtain information about its influence on the flow distribution and the velocity vectors at the exit of the structured foil. To reduce the system by one dimension, it was

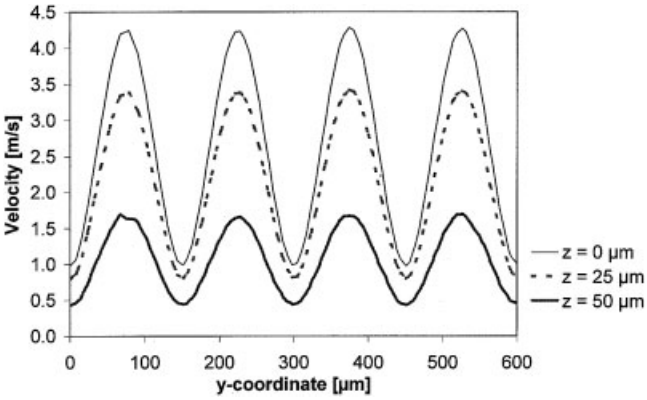

Figure 5. Velocity magnitude at constant heights for 50 μm distance to the channel exits for a total flow of 0.15 L/min STP and 0.05 mm fins between the channels (simulation).

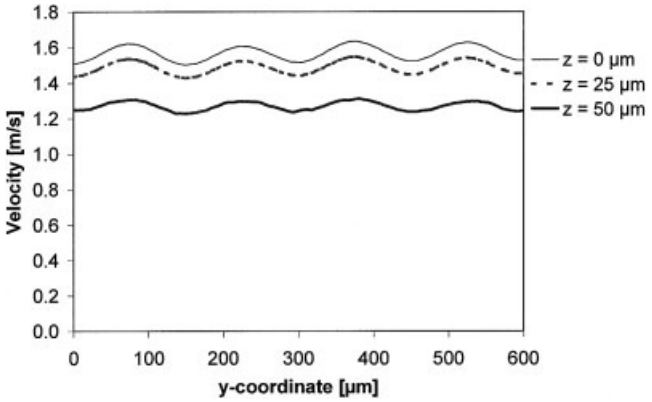

Figure 6. Velocity magnitude at constant heights for 200 μm distance to the channel exits for a total flow of 0.15 L/min STP and 0.05 mm fins between the channels (simulation).

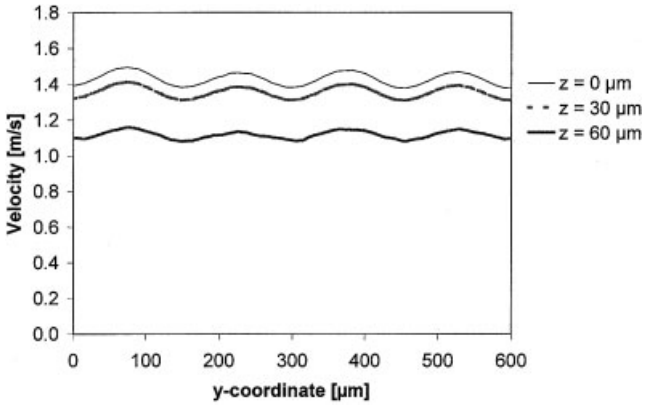

Figure 8. Velocity magnitude at constant heights for 200 μm distance to the channel exits for a total flow of 0.15 L/min STP, 0.05 mm fins between the channels and a 0.01 mm gap above the channels (simulation).

decided to focus on the velocity vectors at half the height of the channels ($z = 0$ μm) where no z-components were observed.

The influence of side walls of the clamping device on the flow distribution over the channel system was observed to be negligible from the simulation. This is an important factor for experimental investigation, since every channel can be treated equally considering the flow outlet effects.

Close to the fluid exits ($x = 0$ μm) the velocity vectors in proximity to the fins always display strong y-components (Figure 3). As a result, the magnitude and direction of the velocity is already independent from the y-position at a distance greater than 200 μm from the fluid exits. The total volume flow, varied from 0.15 to 0.5 to 0.75 L/min STP, has only a minor influence on the velocity vectors at 100 and 200 μm. The variation of velocity with the y-position at 200 μm distance is slightly more pronounced at the higher flow rate.

Additional simulations were performed with 0.2 mm (instead of 0.05 mm) fins between the channels (Figure 4). This is equivalent to every other channel being completely blocked in the standard setup. The zero flow observed between the channels at $x = 100$ μm indicates that it would be possible to detect a blocked channel unanimously. An equivalent statement is that there is also no interference in the maximum of the velocity magnitude from one channel to the adjacent channel.

Due to the fact that the hot wire is long compared to the channel height, it was also expected that the values of the voltage signal are not corresponding to the former plotted velocity vectors. An approach to the experimental values is represented by Figure 5 and 6 where the velocity magnitudes at different z-positions are plotted against the y-position for a distance of 50 and 200 μm from the foil respectively (again, standard geometry). For the lower distance the absolute maximum of the velocity magnitude decreases very fast with increasing z-coordinate, but the minimum in the middle of two channels remains nearly constant even though $z = 50$ μm is parallel to the upper wall of the channels. For the greater distance both values decrease with the same rate. Tendencies can be understood due to the direction of the velocity vectors in proximity to the channel walls.

Taking into account the finite wire length in the experiments, a greater ratio of minimum to maximum velocity values can be expected at distances lower than $x = 200$ μm. Due to flow

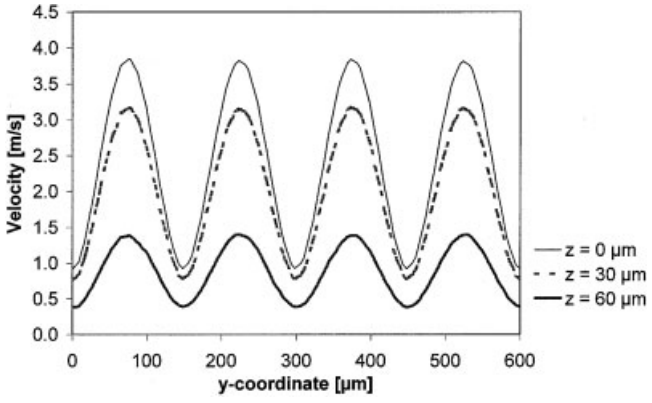

Figure 7. Velocity magnitude at constant heights for 50 μm distance to the channel exits for a total flow of 0.15 L/min STP, 0.05 mm fins between the channels and a 0.01 mm gap above the channels (simulation).

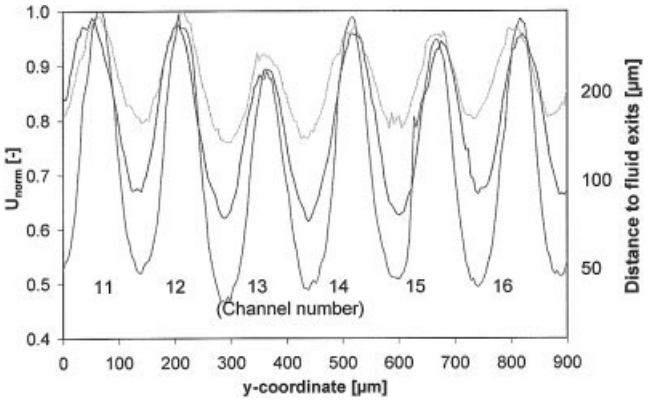

Figure 9. Normalized current vs. y-coordinate for different distances to the channel exits of an uncoated foil (anemometry).

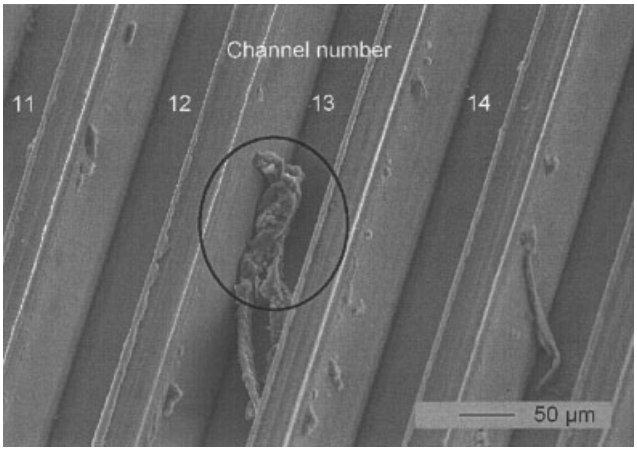

Figure 10. SEM picture of region of the uncoated foil examined by anemometry in Figure 9.

distribution in the z-direction the experimental minimum- maximum ratio should be closer to simulation at $z = 0$ μm for greater distances to the channel exits.

A final simulation examines the influence of gas streams bypassing the foil. The stack was only clamped so that the gas can, for example, leave the system above the fins (small burrs due to diamond cutting of the structure), or even between the unstructured and uncoated (blank) foil and the spacer block. A gap of 0.01 mm was assumed which could be within the experimental error above the fins. Due to the gap assumption the symmetry was only valid in relation to the y-plane, and the cell system was improved by reducing the size of the cells dramatically. The tendencies observed from this simulation (Figures 7 and 8) were the same as for the dependence on the z-coordinate (values for z were chosen slightly different to Figures 5 and 7 due to the additional gap, resulting in a greater channel height). A gap will even out the values of the velocity magnitude at very short distances due to a decreasing maximum, and the influence of the gap on the experiments at greater distances from the foil will be lower.

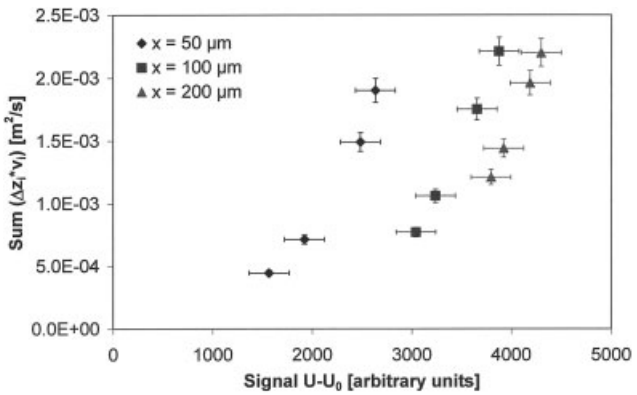

Figure 11. Comparison of measured voltage versus integrated velocity (v×*dz*) derived from laminar modeling at 500 mL/min STP.

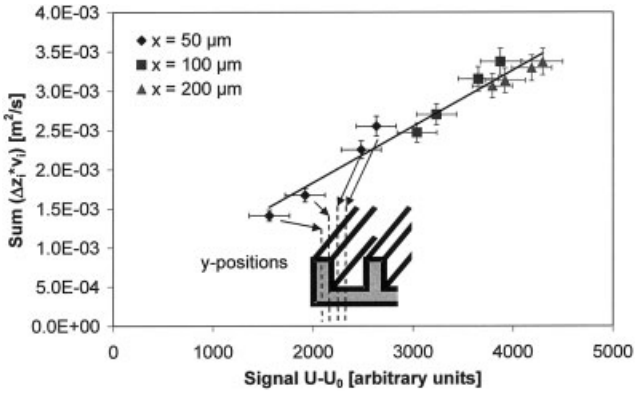

Figure 12. Comparison of measured voltage versus integrated velocity (v×*dz*) derived from turbulent modeling at 500 ml/min STP.

Results from anemometry

The experiments were started with an uncoated structured foil for comparison of the voltage signals with the simulation values. Therefore, the total flow was varied first in the region 0.05 to 1.0 L/min STP to examine the best measurement conditions. Volume flows less than 0.5 L/min STP resulted in very small voltage changes so that the signal-to-noise ratio was poor. With 1.0 L/min STP a time-dependent fluctuation was observed, indicating a high turbulent flow in the outlet region. 0.5 L/min was hence chosen as standard flow.

The first observation with this volume flow was that the overall voltage difference to zero flow doubled when the distance to the fluid exits was increased from 50 to 500 μm in a nonlinear manner. Surprising at first sight, this was understood when taking into account the finite length of the wire. Usually, the whole wire is smaller than the examined flow region and is cooled at its full length. Here, in contrast, the length of the cooled zone is increasing with increasing distance to the fluid exits. At higher distances, the flow velocity will be smaller, but the cooling zone will be longer, which may result in a higher voltage.

Another observation was that the zero flow voltage signal decreased with increasing distance to the foils with a higher gradient closer to the fluid exits. The voltage value at 500 μm

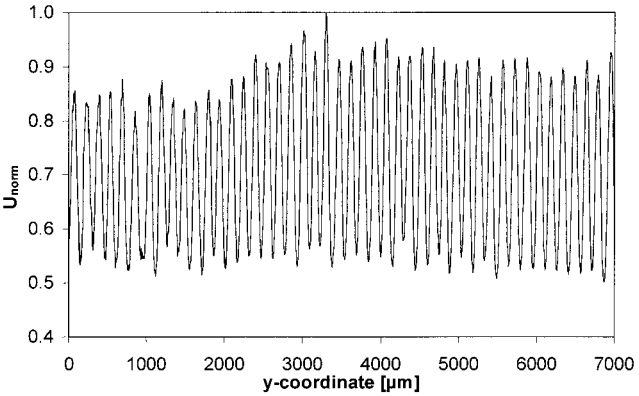

Figure 13. Normalized voltage versus *y*-coordinate for 100 μm distance to the channel exits of sample A (anemometry).

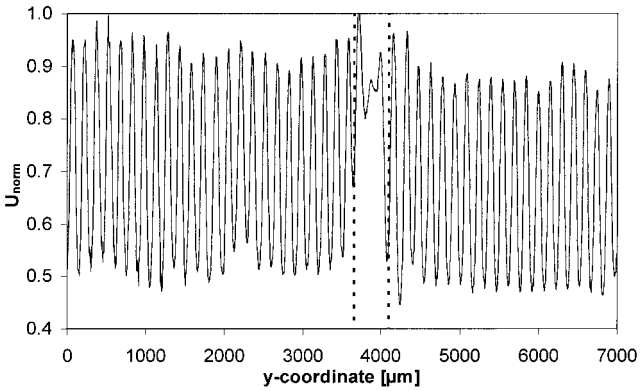

Figure 14: Normalized voltage vs. *y*-coordinate for 100 μm distance to the channel exits of sample B (anemometry).

distance was only 90% of that of the value at 50 μm, the absolute difference being comparable to the offset turning on the gas flow at a distance of 50 μm. The effect can be explained by a heat exchange due to diffusive heat transfer which is known to be a source of error for the determination of velocity profiles in the proximity of fluid walls (Durst and Zanoun, 2002). Radiative heat transfer is negligible at that wire temperature (Durst and Zanoun, 2002).

The normalized voltage is plotted against a chosen *y*-coordinate (channel numbers listed additionally) in dependence of the distance from the foil in Figure 9. The ratio of minimum to maximum value of U_{norm} at $x = 50$ μm (0.5) is greater than that predicted by the simulation plots (such as Figure 5, ratio of minimum to maximum velocity < 0.5 at every position of z). Apart from the fact that velocity/flow-calibration of the wire will be considered later, this can be a result of the finite size of the wire or a possible gap between the foils.

The channel No. 13 is an example for regions with a significantly smaller maximum value. An examination with scanning electron microscopy (SEM) revealed the presence of turnings combined with contaminations (Figure 10).

To link the simulation section and the experimental results,

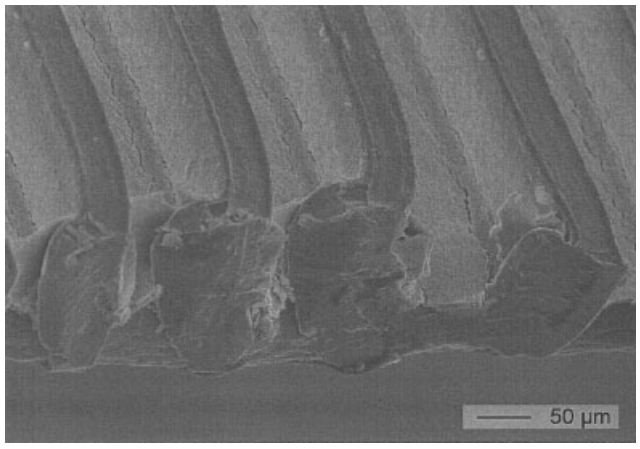

Figure 15. SEM picture of the region between the dotted lines of Figure 14 for sample B examined by anemometry.

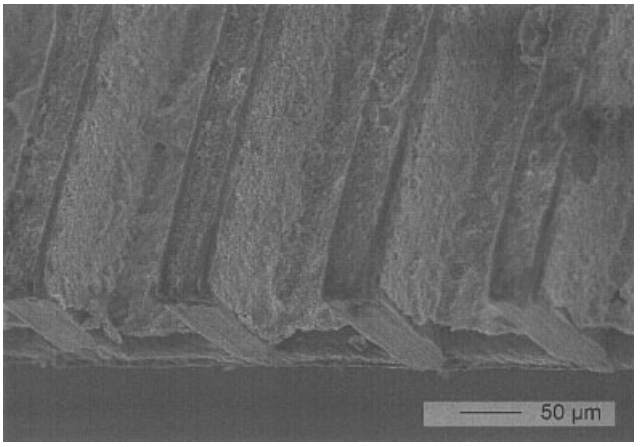

Figure 16. SEM picture of a small representative region of sample A examined by anemometry in Figure 13.

the latter being considerably influenced by the cooled wire length, it was decided to compare laminar and k-ϵ RNG simulation data with results obtained from a clean microchannel foil at 500 mL/min STP. The necessary procedure was, therefore, to integrate the simulated velocity magnitude along the wire length at different positions of *y*, assuming a centered wire position around z = 0 μm. A comparison of the integrated velocity values from the laminar and turbulence model with measured voltages $U(y)$-U_0 at three positions of x and four positions of y each, can be found in Figures 11 and 12, respectively. The four positions of y are the projection of the middle, of the quarter and of the wall of the channel, as well as of the middle of the fin at different positions of x. Considering experimental and simulation error, it can be concluded that the k-ϵ RNG model describes the system well, whereas with the assumption of laminar flow at the channel exit, clearly no linear relation between cooling and flow is obvious.

For the scanning procedure of the coated samples A–E to determine the homogeneity of the layer thickness, a distance to the fluid exits of 100 μm was chosen. Figures 13 and 14 show the normalized voltage signal against the travel distance of the

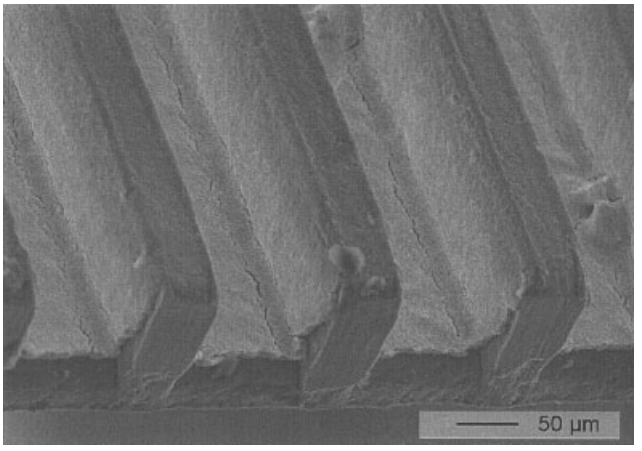

Figure 17. SEM picture of a small representative region of sample B examined by anemometry in Figure 14.

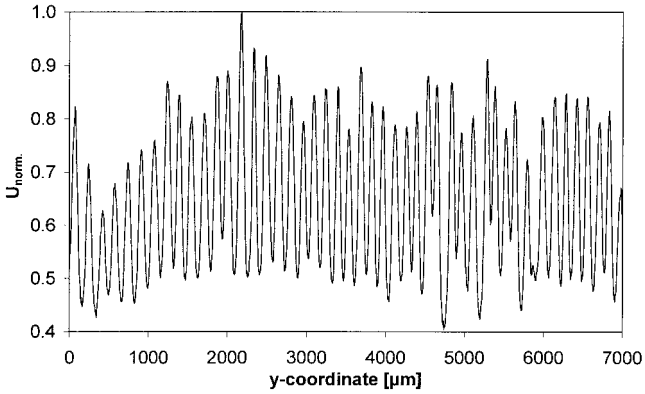

Figure 18. Normalized voltage vs. y-coordinate for 100 μm distance to the channel exits of sample D (anemometry).

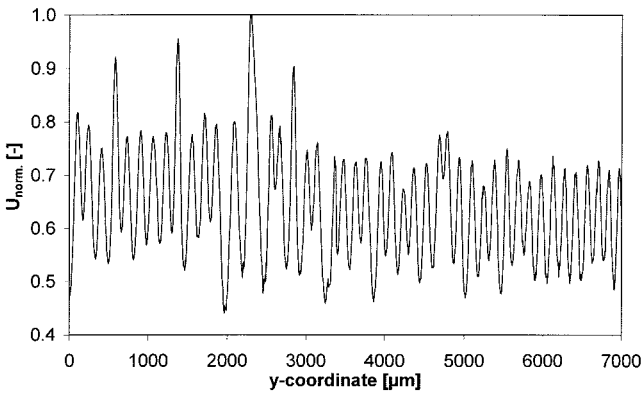

Figure 20. Normalized voltage vs. y-coordinate for 100 μm distance to the channel exits of sample E (anemometry).

wire for sample A and B, respectively. The distribution of the maximum values is better for sample B, except for the region between the dotted lines for Figure 14, where a cutting defect influenced the voltage signal (SEM picture in Figure 15). The median values are 0.897 $\pm$ 0.044 for sample A and 0.917 $\pm$ 0.037 for sample B. The ratio of minimum to maximum values are always around 0.5, and are higher compared to the structured foil (0.7 at x = 100 μm) due to the coating of the channels and the resulting smaller diameter increasing the fluid velocity.

SEM pictures (Figure 16 and 17) of the different coatings clarify the tendencies observed by anemometry. The smaller size of the nanoparticle agglomerates (see Pfeifer et al., 2002) in the dispersion of sample B causes a smoother surface and better thickness distribution.

The deviation of the voltage signal for the additional sample C was a little bit higher than that of sample A, which was supposed from the increase in layer thickness from sample A to C. The voltage signal was 0.874 $\pm$ 0.070.

Apart from the latter results, a deeper impression of the applicability of hot wire anemometry for flow characterization in microchannels can be derived from more inhomogeneous coatings such as samples D and E. Sample D was chosen in order to show the effects of agglomerate sizes greater than 1 μm on the flow distribution, because 3 h of dispersing with the magnetic stirrer is too short to isolate the nanoparticles by shearing. For sample E, a drying temperature as high as 90°C during the washcoating with a HEC/water dispersion, was known to decrease the homogeneity of the forming layer by building bridges from one fin to the adjacent fin. The voltage signals and the corresponding SEM-pictures are shown in the Figures 18–21. The statistic analysis is summarized in Table 2.

To obtain information on the deviation in volume flow from the statistic analysis of the voltage signal, calibrations were performed with the different samples at a representative channel (at median normalized voltage) for different positions of x and y in the flow range from 300 to 700 ml/min STP. It was shown that a simple fit of the experimental data could be applied in that way

$$U - U_o = a\dot{V} + b \tag{2}$$

for all volume flows at constant position, and that a was nearly constant for all data derived from one y-position but different

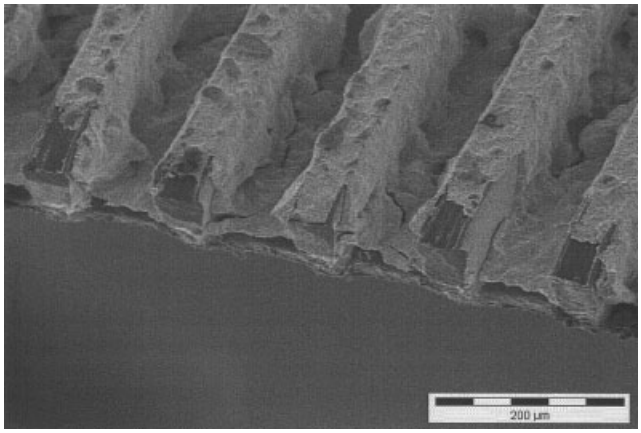

Figure 19. SEM picture of a small representative region of sample D examined by anemometry in Figure 18.

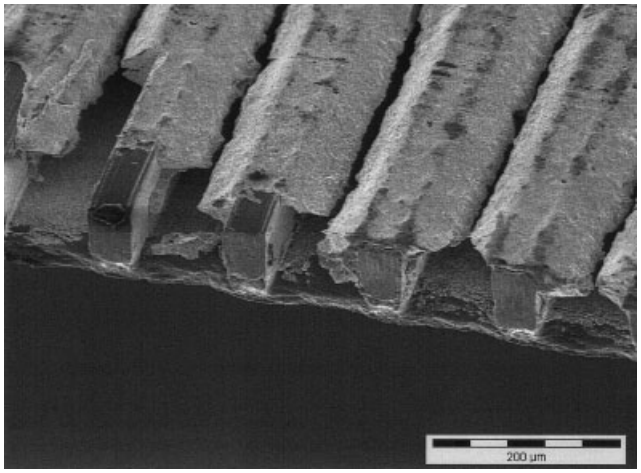

Figure 21. SEM picture of a small representative region of sample E examined by anemometry in Figure 20.

Table 2. Results from Anemometry for the Different Catalyst Layer Preparations and the Uncoated Foil

Sample	Median Norm. Voltage [−]	Deviation Voltage	Standard Dev. Volume Flow, %	Maximum Dev. Volume Flow, %
Uncoated	0.980	0.032	6.6	15.9
A	0.897	0.044	9.3	18.6
B	0.917	0.037	7.7	15.3
C	0.874	0.070	14.8	22.2
D	0.821	0.086	18.8	30.0
E	0.764	0.090	20.9	31.5

x-positions (50-200 μm). The gradient a was always low so that even small values of voltage deviation give higher volume flow deviations (the results are summarized in Table 2). While the standard samples A to C yield flow deviations below 15% (maximum 22%), the standard flow deviation for the inhomogeneous coatings are even higher than 20% with a maximum of 31.5%.

Additional information about the flow distribution at the flow exit of the microchannels can be obtained from a closer look, such as in Figure 20. Whenever a very high or low minimum voltage signal (middle of fin) is found, the maximum voltage signals (middle of channel) are closer to or further from each other, respectively. This can be traced to disturbed flow by different layer thickness at different channel walls. However, this is a more qualitative evaluation of the voltage signal and can help support the statistical analysis of flow deviation between the channels of a structured foil.

Conclusion and Outlook

The simulation of the fluid flow at the exit of the microchannels has shown that it is possible to measure the maximum fluid velocity of adjacent channels without mutual interference at a maximum distance from the fluid exits of 100 μm. The fins that separate the channels must only be 0.05 mm wide.

Hot wire anemometry was proven to be an excellent technique for quantification of the fluid flow distribution when precise positioning of the wire is guaranteed. Effects due to stream divergence on the voltage signal of the anemometer have to be considered for interpretation of the results. Gaps between the structured foils can have a strong influence on the voltage signal. The effects quantified by anemometry are transferable to catalyst tests and, therefore, offer the opportunity to characterize the quality of the coatings, or manufacturing tolerances of micro-components, respectively.

Presently, the method is restricted to a 1-D (one-dimensional) array of channels. Future work may be aimed at extending it to 2-D arrays, such as multistack microstructures or honeycombs, respectively.

Notation

a,b = coefficients of fit, Vs/m^3, V
U_{norm} = normalized voltage
$U(y)$ = measured voltage at position y (constant x,z-position), V
U_0 = measured voltage without fluid flow at constant x,z-position, V
U_{max} = measured maximum voltage with fluid flow at constant x,z-position, V
v = velocity magnitude, m/s
$\dot{V}$ = volume flow, m^3/s

Literature Cited

Ajmera, S. K., C. Delattre, M. A. Schmidt, and K. F. Jensen, "A Novel Cross-Flow Microreactor for Kinetic Studies of Catalytic Processes," *Proc. of 5th Int. Conf. on Microreaction Technol.*, Strasbourg, France, 414 (May 27–30, 2001).

Bier, W., W. Keller, G. Linder, D. Seidel, and K. Schubert, "Manufacturing and Testing of Compact Micro Heat Exchangers with High Volumetric Heat Transfer Coefficients," *Microstructures, Sensors, and Actuators.* , **19**, 189 (1990).

Commenge, J. M., L. Falk, J. P. Corriou, and M. Matlosz, "Optimal Design for Flow Uniformity in Microchannel Reactors", *AIChE J.,* **48**, 345(2002).

Durst, F., and E. S. Zanoun, "Experimental Investigation of Near Wall Effects on Hot-Wire Measurements", *Experiments in Fluids*, **33**, 210 (2002).

Fichtner, M., W. Benzinger, K. Haas-Santo, R. Wunsch, and K. Schubert, "Functional Coatings for Microstructured Reactors and Heat Exchangers", *Proc. of 3rd Int. Conf. on Microreaction Technol.*, Frankfurt, Germany, 372 (April 18–21, 1999).

Howitt, J. S., and T. C. Sekella, "Flow Effects in Monolithic Honeycomb Automotive Catalytic Converters", *Automotive Engineering Congress*, Detroit, MI, Society of Automotive Engineers (*SAE) paper No. 740244,* Warrendale, PA (1974).

Pfeifer, P., M. Fichtner, K. Schubert, M. A. Liauw, and G. Emig, "Microstructured Catalysts for Methanol-Steam Reforming", *Proc. of 3rd Int. Conf. on Microreaction Technol.*, Frankfurt, Germany, 372 (April 18–21, 1999).

Pfeifer, P., O. Görke, and K. Schubert, "Washcoats and Electrophoresis with Coated and Uncoated Nanoparticles on Microstructured Metal Foils and Microstructured Reactors," *Proc. of 6th Int. Conf. on Microreaction Technol./AIChE Spring Meeting*, New Orleans, 281 (March 10–14, 2002).

Schubert, K., W. Bier, J. Brandner, M. Fichtner, C. Franz, and G. Linder, "Realisation and Testing of Microstructure Reactors, Micro Heat Exchangers and Micromixers for Industrial Applications in Chemical Engineering", *Proc. of 2nd Int. Conf. on Microreaction Technol./AIChE Spring Meeting*, New Orleans, 8 (March 8–12, 1998).

Wegeng, R. S., M. K. Drost, and D. L. Brenchley, "Process Intensification Through Miniaturisation of Chemical and Thermal Systems in the 21st Century", *Proc. of 3rd Int. Conf. on Microreaction Technol.*, Frankfurt, Germany, 2 (April 18–21, 1999).

Manuscript received Jan. 17, 2003, revision received Jun. 27, 2003, and final revision received Aug. 10, 2003.